Contribution from the Department of Chemistry,
University of Pittsburgh, Pittsburgh, Pennsylvania 15260

Study of the Crystal Field Interaction in $NdAl_3$ by Measurement of Heat Capacity, Susceptibility, and Resistivity

J. V. MAHONEY, W. E. WALLACE,* R. S. CRAIG, and S. G. SANKAR

Received March 11, 1975 AIC50184K

Heat capacity, electrical resistivity, and magnetic susceptibility of $NdAl_3$ have been measured over the temperature range 4–300 K. The results are used to elucidate the influence of the hexagonal crystal field in $NdAl_3$ on the $^4I_{9/2}$ ground-state multiplet of the Nd^{3+} ion. Measurements indicate that the crystal field interaction is stronger than exchange but the latter is sufficient to produce antiferromagnetic ordering below 4 K, primarily within a Γ_8 doublet state. Using a Hamiltonian with second-, fourth-, and sixth-order terms three sets of crystal field parameters are obtained which are in reasonable accord with experiment. Examination of the crystal field intensity parameters in the context of the point charge model seems to indicate that nonelectrostatic terms are significantly involved in the crystal field interaction. As an aid to the general analysis, heat capacity measurements were made on $Nd_{0.4}La_{0.6}Al_3$.

I. Introduction

Numerous studies have been made in this laboratory in recent years dealing with the influence of the crystal field (CF) interaction on the behavior of rare earth intermetallics.[1] The CF interaction has been shown to influence the bulk magnetic properties (susceptibility, etc.), heat capacity (C_p), and electrical resistivity (ρ). By studying the temperature dependence of susceptibility (χ), C_p, and ρ it has often proved possible to elucidate many of the details of the CF interaction.

Indeed, this wide variety of experimental data is certainly necessary if accurate parametrization of the CF interaction is to be achieved. Previous modeling has been largely based upon the simplified point charge–single ion concept. It should be pointed out, however, that although this model seems to be satisfactory in some important cases,[2,3] its utility is not universal among the metallic rare earths. There have, in fact, been a number of studies[4,5] in which the experimentally determined CF parameters cannot be explained within the confines of the purely electrostatic interaction model. These discrepancies point out the desirability of more extensive studies of the CF interaction in metallic rare earth systems.

The present paper constitutes the third in a series of reports dealing with the CF effects in RAl_3 compounds with R = Ce, Pr, and Nd. These crystalline materials provide the unique opportunity of studying an isostructural system in which the CF interaction is either the sole or predominant factor involved in determining the thermal dependence of the macroscopic properties referred to above. The most simple case is exemplified by $PrAl_3$[6] in which the nonmagnetic ground state, giving rise to Van Vleck paramagnetism, is induced solely by the CF interaction. A more complicated situation is presented by $CeAl_3$[7] where the experimental data reflect the combined effects of CF and Kondo interactions. Finally, measurements on $NdAl_3$ are reported in this communication. As in the previous two RAl_3 cases, we find the CF effects to be the predominant influence on the measured properties. However, in this case exchange is stronger as is evidenced by the appearance of antiferromagnetic ordering below 4 K. As will be demonstrated, parameters appropriate to the description of the CF interaction can be calculated on the basis of the presented data. For this purpose we rely mainly upon heat capacity measurements since the CF parameters are most accurately determined from these data. The resistivity measurements, although of quantitative value, cannot be rigorously applied to CF parameter calculations because of the difficulty in obtaining a suitable estimate of the phonon and residual contributions to the measured ρ and in separating these from the spin-disorder term; the latter is the contribution which is affected by the crystal field interaction. This inability to separate the contributions is unfortunate, for the calculated spin-disorder resistivity possesses a strong eigenfunction dependency (see eq 10) and is potentially of great utility in determining the correct CF parameters.

The results of susceptibility experiments have been presented primarily to provide information in regard to the magnetic interactions in $NdAl_3$. As has been pointed out elsewhere,[6] for temperatures above 10 K the calculation of polycrystalline susceptibilities is in most cases rather insensitive to the choice of CF parameters. This is indeed the situation in $NdAl_3$, as is shown in Figure 3.

In regard to the magnetic properties of $NdAl_3$, our results are at variance with those obtained in an earlier study of Buschow and Fast.[8] They observed the susceptibility to behave in a typical Curie–Weiss manner for temperatures in excess of 60 K. Below this temperature, however, significant deviations were observed which could not be explained on the basis of magnetic ordering, CF effects, or a combination of these effects. We can only conclude from the relatively straightforward behavior of our samples (see Figure 3 below) that this previous work was conducted on impure multiphase material.

II. Experimental Section

The rare earth starting materials had a stated 99.9 wt % purity with respect to other lanthanides. With the exceptions of La and Sm (approximately 0.03 wt %) all other rare earth impurities either were not detected or were less than 0.01 wt %. The crucible material during the purification process was Ta and represented less than 0.8%, while all other detectable elements were evident in amounts less than 0.01 wt % (Si, Fe, Mg, Ca, and Al). No attempt was made to analyze the quantities of the gaseous impurities. The stated purity of the aluminum starting material was 99.999 wt %.

Using induction heating and a water-cooled copper boat, the elements were melted together under a purified argon atmosphere to form the compound. By limiting each ingot to an approximate mass of 6 g, this technique provided melts which could be maintained for a period of 1 or 2 min with vigorous stirring and virtually no contamination from the cold boat. The resulting heat treatment was found to be important for the formation of single-phase samples. The optimal conditions consisted of annealing the samples which had been wrapped in tantalum in an argon atmosphere for a period of 3 weeks at 800°C. Nearly 80 g of $NdAl_3$ and 6 g of $Nd_{0.4}La_{0.6}Al_3$ were prepared in this manner. X-Ray powder diffraction measurements showed both compositions to be single phase within the limits of this analytical method (approximately 4%).

Heat capacity data were obtained employing two adiabatic calorimeters operating in overlapping temperature ranges. Between 15 and 300 K we feel justified in claiming an accuracy of nearly 0.2% as has been determined by measurements of a National Bureau of Standards sample of benzoic acid. In the lower temperature range (2–15 K) our accuracy has been established as about 1%. More details of these measurements and instruments have been given elsewhere.[9,10]

The resistivity was measured on an elongated bar ($\sim$1 cm × 2 mm^2) by the familiar four-terminal dc method, while the susceptibility data were obtained by the Faraday technique employing a powdered sample. Both types of measurements were repeated on separate samples to

ensure results characteristic of $NdAl_3$. The reproducible nature of these data indicated that the prepared ingots represented well-homogenized low-impurity materials.

III. The Crystal Field Hamiltonian

The customary Hamiltonian, based upon a "one-particle potential", used to describe the CF interaction in rare earth systems is[11]

$$\mathcal{H}_{CF} = \sum_{n=0}^{\infty} \sum_{m=+n}^{-n} B_n^M O_n^m \qquad (1)$$

The quantities O_n^m are the well-known Stevens operator equivalents which are provided in terms of the total angular momentum operators. O_n^m is dependent only on the ground-state multiplet of the rare earth ion. The angular dependence and thus the description of the strength and nature of the CF interaction are contained in the coefficients B_n^m. This form of the Hamiltonian is general to the extent that it is developed from a potential equation which in no way restricts the nature of the charge distribution of the surrounding environment. Very often in the literature, however, attempts are made to place significance on the coefficients B_n^m with the help of the "point-charge model". It is within the confines of this model that the nature of the interaction is strictly defined. It should be noted that the operator-equivalent technique (embodied in eq 1) of treating the CF interaction is valid only for calculations in which J is "a good quantum number", i.e., the case in which the CF perturbation is small compared to the energy difference between the multiplets. For the purposes of the present study this restriction represents no loss of generality since the $J = {}^9/_2$ ground multiplet of Nd^{3+} lies nearly 3000 K below the first excited ($J = {}^{11}/_2$) multiplet.

The number of nonvanishing terms in eq 1 becomes manageable by considering the site symmetry of the rare earth ion. The characteristic crystalline structure of the "light" RAl_3 compounds is the Ni_3Sn type.[12] With the axis of quantization along the hexagonal c axis, the point symmetry at the rare earth site is D_{6h} and eq 1 reduces to

$$\mathcal{H}_{CF}(NdAl_3) = B_2^0 O_2^0 + B_4^0 O_4^0 + B_6^0 O_6^0 + B_6^6 O_6^6 \qquad (2)$$

In this equation the coefficients are connected to the familiar parameters[6,13] W, x, and y by the defining relations

$$B_2^0 = \frac{(1 - |y|)W}{F_2}$$

$$B_4^0 = \frac{xyW}{F_4}$$

$$B_6^0 = \frac{(1 - |x|)yW}{F_6}$$

$$B_6^6 = M_6^6 B_6^0$$

The numerical factors F_2, F_4, and F_6 have been conveniently tabulated,[14] while M_6^6 can be easily calculated. The general effect of the CF interaction in $NdAl_3$ is that the tenfold degenerate ground-state multiplet $^4I_{9/2}$ is split into five Kramer doublets. By diagonalizing the matrix corresponding to the Hamiltonian in eq 2, the eigenvalues and eigenfunctions for various values of W, x, and y are obtained.

IV. Results and Discussion

Our determination of the Schottky and magnetic heat capacity contributions in the RAl_3 compounds is based upon the assumption that the phonon and electronic components are suitably estimated by the measured heat capacity of the isostructural, nonmagnetic $LaAl_3$. This assumption has been thoroughly considered and justified for $PrAl_3$ in a previous paper.[7] The same considerations would appear to apply to $NdAl_3$. Proceeding on this assumption our measurements indicate that we account for about 94% of the expected

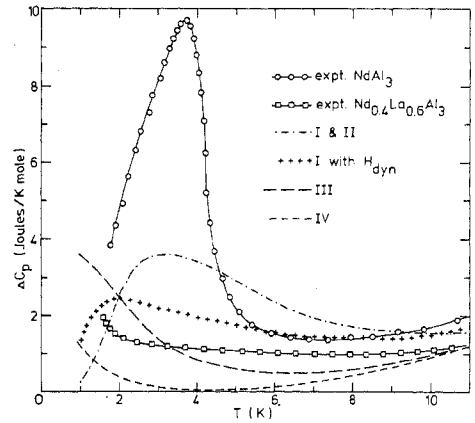

Figure 1. Comparison of the experimental excess heat capacity of $NdAl_3$ and $Nd_{0.4}La_{0.6}Al_3$ (between 1 and 11 K) with the calculated CF-only contribution for each of the proposed schemes. The modification when dynamical exchange (see text) is included is also shown.

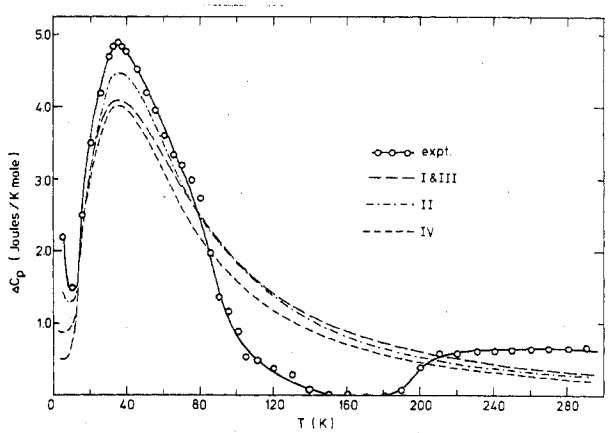

Figure 2. Comparison of the measured and calculated crystal field heat capacities for $NdAl_3$ between 6 and 300 K.

magnetic and CF entropy [R ln $(2J + 1)$]. The actual heat capacity data are presented in Figures 1 and 2, for the temperature ranges 1.8–11 and 5–300 K, respectively. In both of these figures the results are presented as the excess heat capacity of the neodymium-containing compound over that of nonmagnetic $LaAl_3$. For $NdAl_3$ two well-separated and distinct maxima are observed, at 3.7 and 35 K.

Although the shape of the lower temperature peak is not that of a usual λ anomaly, it can nonetheless be concluded (see the χ values in Figure 3) that it results from an antiferromagnetic order–disorder transition, which is occurring primarily within the ground-state CF doublet. Such a process leads to a Zeeman splitting of this doublet and thus to an associated theoretical entropy of R ln 2 or 5.77 J/(K mol). The entropy connected with this experimental peak, however, amounts to almost 8 J/(K mol). This clearly indicates additional contributions arising from thermal excitations into a low-lying CF state.

At this point we note that the convention followed in the several diagrams is that experimental results or data obtained from experimental measurements are represented in the figures as solid lines. Where appropriate, data points are included but usually not in their entirety. Calculated results are represented as some form of broken line.

In an attempt to clarify the origin of the unusual shape of the 3.7 K anomaly, measurements were performed on the compound $Nd_{0.4}La_{0.6}Al_3$. It is supposed that the substitution of nonmagnetic lanthanum for neodymium suppresses the exchange interaction and therefore lowers the Néel temperature, without appreciably altering the crystal field effects.

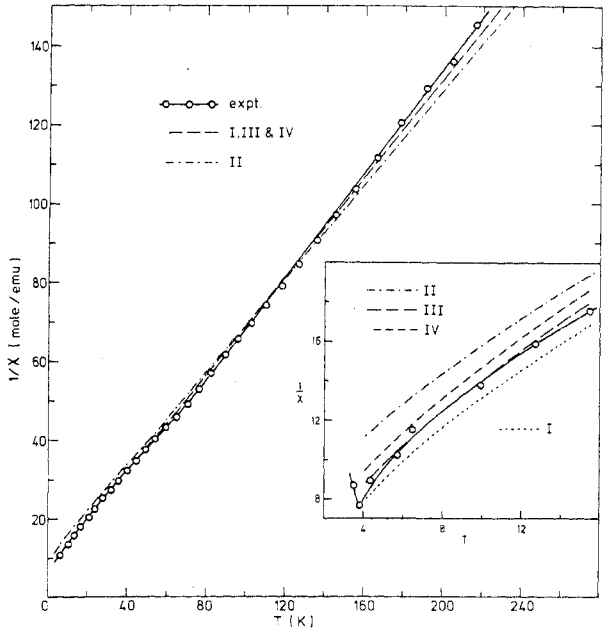

Figure 3. Inverse susceptibility per mole vs. temperature for $NdAl_3$. The calculated quantities have already been adjusted for the "best fit" values of the molecular parameter indicated in Table I.

The results for the ternary system, shown in Figure 1, indicate that the Néel temperature is somewhat below 1.7 K. However, the magnitude of ΔC_p for the ternary system indicates that there is an appreciable contribution to the heat capacity in the temperature region originating from the population of higher CF states. It is probably this which confers the unusual shape on the 3.7 K anomaly and gives rise to the excess entropy above R ln 2. It then becomes necessary to describe the low-temperature properties of $NdAl_3$ in terms of a crystal field interaction which provides a first excited doublet roughly 10 K above the ground state.

The distribution of the higher CF states is mainly determined by a least-squares fitting of the information presented in Figure 2. The maximum occurring at 35 K is a characteristic Schottky anomaly and results from the thermal population of higher CF states as temperature increases. An important feature of this peak is the prolonged tail on the high-temperature side, which indicates that the overall splitting of CF states is in excess of 100 K. The rapid drop in ΔC_p to zero at 140 K and the subsequent continuation of measurable quantities above 185 K is a troublesome feature complicating the analysis; these complications are probably the consequences of the imperfection of the assumption that C_p for $LaAl_3$ properly represents the electronic and phonon contributions for $NdAl_3$. Even so, the temperature region of major interest, between 0 and 100 K, contains, as noted above, over 90% of the maximum possible entropy of R ln $(2J + 1)$. Thus the failure of ΔC_p to decrease smoothly to zero above 100 K should have only a small effect on the outcome of the fitting procedures.

The results of magnetic measurements are shown in Figure 3 as inverse susceptibility vs. temperature. Although these measurements indicated nearly free ion behavior at high temperatures, below 60 K small positive deviations from Curie–Weiss behavior were observed. This anomalous behavior persisted down to the Néel temperature, ~4 K. The effective moment of 3.45 μ_B, calculated from the linear portion of the curve, compares favorably with the theoretical value of 3.62 μ_B.

The resistivity results are shown in Figure 4. It is obvious that for temperatures above 100 K the usual linearly temperature dependent phonon scattering term is the principal contribution to the resistivity. In this region the contribution arising from the paramagnetic scattering or spin-disorder resistivity is nearly temperature independent. This is the situation when the Boltzmann factors are essentially equal for all CF states and the several states are populated statistically by the ions in the assembly.[15] At lower temperatures, however, the Boltzmann population factors are different for the several states and hence their populations vary significantly with temperature. This variation of population with temperature means that the spin-disorder contribution is temperature dependent, which leads to the noticeably nonlinear measured resistivity. The paramagnetic scattering of the conduction electrons is mainly responsible for the large values of resistivity down to low temperatures. The abrupt drop in the experimental values near 4 K is characteristic of the rapid decrease in this spin scattering of the conduction electrons accompanying the onset of magnetic order.

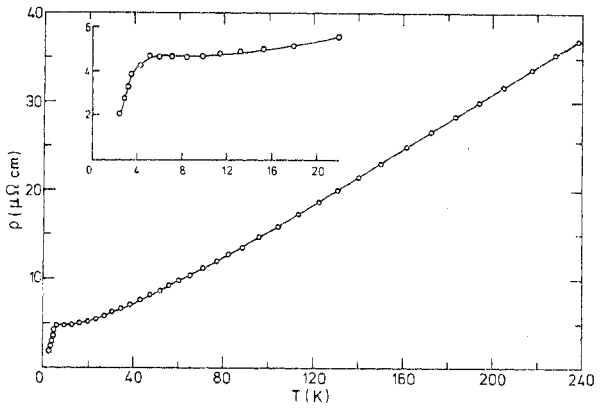

Figure 4. Total measured resistivity for $NdAl_3$.

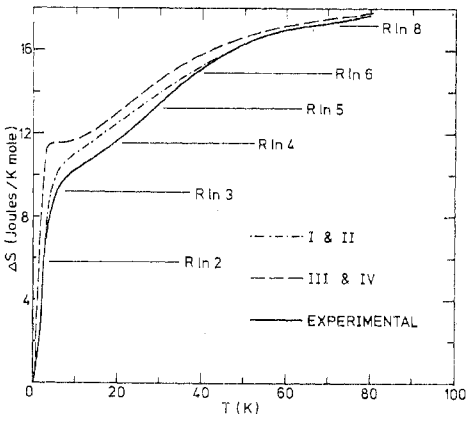

Figure 5. Calculated and experimentally determined thermal response of the excess entropy for $NdAl_3$.

The calculation of appropriate eigenvalues and eigenfunctions according to eq 2 is greatly facilitated by first considering the thermal response of the magnetic entropy. This information can be derived from our heat capacity data and, as has been indicated, should eventually reach the value R ln 10 at high temperature. At lower temperatures, the magnetic entropy will have a sensitive dependence on the CF eigenvalues through a Boltzmann-type relationship and, therefore, can often yield some valuable information about the lower energy CF states. Figure 5 is a plot of this excess entropy as a function of temperature between 0 and 80 K. Of particular interest is the rapid increase of ΔS from lowest temperature to 12 K. The rapid accumulation of R ln 2(3 K) is, of course, the result of the antiferromagnetic order–disorder transition. That this buildup of entropy should continue and, in fact, reach R ln 3 by 5 K leads, as noted above, to the conclusion that

Table I. Crystal Field Parameters for $NdAl_3$

Scheme	Crystal field coefficients			Best-fit molecular field parameter, $-\lambda$, emu/mol
	W, K	x	y	
I	16.3 ± 1.1	0.20 ± 0.05	0.35 ± 0.04	3.0 ± 1
II	−15.1 ± 1.3	−0.20 ± 0.08	0.36 ± 0.04	6.0 ± 2
III	−6.6 ± 0.6	0.07 ± 0.03	0.85 ± 0.06	4.0 ± 1
IV	6.2 ± 0.6	−0.10 ± 0.03	0.93 ± 0.07	5.0 ± 1

the first excited CF doublet must be in the vicinity of 10 K. In addition, the splitting between the ground state and the most excited state appears to be of the order of 100 K, as is indicated by the significant entropy being added near 80 K. Placing these two conditions upon the solutions of eq 2 greatly reduces the number of acceptable sets of CF parameters (W, x, y). These parameters can then be refined by using a least-squares fitting procedure of the heat capacity and susceptibility data. Equation 3 describes the functional dependence of the Schottky

$$C_{CF} = \left[R/T^2 \sum_{i=1}^{n} \left(g_i E_i^2 e^{-E_i/T}/Q\right) - \left(\sum_{i=1}^{n} g_i E_i e^{-E_i/T}/Q\right)^2\right] \quad (3)$$

heat capacity upon the eigenvalues. Here, g_i represents the degeneracy of the ith CF state, E_i is the energy in kaysers, and Q is the partition function. R and T are, of course, the gas constant and temperature, respectively. This relationship has the feature that the shape and temperature position of the calculated Schottky maximum are very sensitive to the eigenvalues E_i and thus to W, x, and y. For the calculation of the polycrystalline susceptibilities, we consider the effect of the applied field to be a small perturbation on the CF-only states. In the small-field approximation the susceptibility is given by the general formula[16]

$$\chi = (g^2\mu_B^2/kT)\left[\left(\sum_{\substack{n,m \\ (E_n=E_m)}} J_{nm}^2 e^{-E_n/kT}/Q\right) - \left(\sum_n J_n e^{-E_n/kT}/Q\right)^2\right] + 2g^2\mu_B^2 \sum_{\substack{n,m \\ E_n\neq E_m}} \frac{J_{nm}^2}{E_m - E_n} e^{-E_n/kT}/Q \quad (4)$$

Here g is the Landé factor for the rare earth ion and the J_{nm} are the matrix elements connecting the nth and mth CF states. Because of these matrix elements the calculated susceptibility becomes dependent on the actual form of the CF eigenfunctions, and thus one expects the fitting of such data to be valuable in the determination of appropriate W, x, and y values. Unfortunately, the approximations that are necessary to calculate χ values for polycrystalline samples severely limit the sensitivity of this approach. For the purposes of these powder experiments we must solve eq 4 for both parallel (J_z) and perpendicular (J_x) orientations of the external field with respect to the axis of quantization. The total CF-only susceptibility (χ_{CF}) is then considered to be the following geometrical average of these orientations

$$\chi_{CF} = {}^1/_3\chi_\parallel + {}^2/_3\chi_\perp \quad (5)$$

To compare these values with experiment, suitable allowances of exchange effects are made by employing the molecular field model. The resulting χ_{calcd} includes the familiar paramagnetic molecular field parameter λ and is given by

$$\chi_{calcd} = \chi_{CF}/(1 - \lambda\chi_{CF}) \quad (6)$$

A reasonable estimate of λ is readily obtained by extrapolating the experimental susceptibility to $T = 0$ K and yields the value $\lambda = -4.0$ emu/mol.

The CF parameters resulting from least-squares fitting procedures using eq 2–6 are shown in Table I. For the fitting of the heat capacity data the parameters W, x, and y were varied, while the additional parameter λ must be included for the susceptibility data. The uncertainties shown in the table repesent the limit by which the parameters can be varied without significantly affecting the fit of the experimental data. Major emphasis is placed on the temperature position and shape of the Schottky maximum and on the determined value of λ. The attempt has been made to keep λ_{calcd} very near the value obtained experimentally. It should be sufficient to say that the "next best" set of CF parameter yielded nearly a 20% increase in standard deviation over those sets indicated in Table I. The macroscopic properties calculated according to these schemes are compared with experiment in Figures 1–3. It is important to reiterate that Figure 1 actually presents two sets of experimental data. We have taken the results for $NdAl_3$ to be indicative of the combined effects of CF and exchange interactions between 2 and 5 K. In this same temperature region we have assumed that the data for $Nd_{0.4}La_{0.6}Al_3$ are representative of the CF-only situation, i.e., $C_{CF}(NdAl_3) = 2.5[\Delta C_p(Nd_{0.4}La_{0.6}Al_3)]$. Thus one might be tempted on first sight to question the applicability of schemes I and II since they would give rise to a Schottky maximum near 3.2, whereas no such peak is observed in the lanthanum-containing ternary system. There are, however, two considerations which can be invoked to bring the treatment represented by curves I and II into agreement with experiment: (1) that the replacement of 60% of the neodymium ions by lanthanum does not really leave the CF interaction unaltered as we have assumed; (2) that for $T > T_N$ there is a significant perturbation resulting in some way from the molecular field, i.e., from the interactions of the paramagnetic Nd^{3+} ions. Each of these possibilities has an interesting implication. Since we have observed no structure or significant lattice parameter change between the parent and diluted compound, the first consideration might lead one to believe that the CF interaction in $NdAl_3$ contains significant contributions from nonelectrostatic mechanisms. In the electrostatic description we expect the interchange of two physically and electronically similar ions like Nd^{3+} and La^{3+} will not appreciably change the strength of the interaction, unless there was an altering of the crystal symmetry or interatomic distances. The alternatives to an electrostatic mechanism have been conveniently reviewed[17] and are rapidly gaining increased consideration. If, on the other hand, we accept the second explanation, then we should modify our calculations according to recent suggestions[18] which attempt to account for thermal fluctuations in the expectation value of the total angular momentum operator $\langle\vec{J}\rangle$. These considerations predict a dynamical exchange field H_{dyn} defined by

$$\vec{H}_{dyn} = \lambda g\mu_B(\vec{J} - \langle\vec{J}\rangle) \quad (7)$$

whose probability distribution $[W(H_{dyn})]$ follows the relationship

$$W(H_{dyn}) \approx \exp\left[\frac{-H_{dyn}^2}{2k_BT\lambda}\right] \quad (8)$$

Our new Hamiltonian for $T > T_N$ then becomes

$$\mathcal{H}_{T>T_N} = \mathcal{H}_{CF} - \sum_i g\mu_B\vec{H}_{dyn}\cdot\vec{J}_i \quad (9)$$

Table II. Eigenvalues and Eigenvectors Resulting from the Parameters Indicated in Table I Eigenvector Representation[a]

Scheme	Eigenvectors	Energy, K	Coefficients	B_4^0/B_2^0	B_4^0/B_6^0
I	Γ_9^2	167.4	$a = 0.358$	7.69×10^{-3}	5.25
	Γ_8^2	93.4	$b = 0.934$		
	Γ_9^1	60.8	$c = 0.195$		
	Γ_7	7.7	$d = 0.981$		
	Γ_8^1	0.0			
II	Γ_7	157.9	$a = -0.394$	8.03×10^{-3}	−5.40
	Γ_8^1	82.4	$b = -0.919$		
	Γ_9^1	77.2	$c = -0.296$		
	Γ_9^2	7.6	$d = -0.956$		
	Γ_8^2	0.0			
III	Γ_8^1	129.2	$a = -0.287$	28.32×10^{-3}	3.84
	Γ_7	93.2	$b = -0.958$		
	Γ_9^1	49.3	$c = -0.714$		
	Γ_9^2	2.7	$d = -0.701$		
	Γ_8^2	0.0			
IV	Γ_8^2	125.7	$a = 0.294$	-94.86×10^{-3}	−6.20
	Γ_9^2	97.1	$b = 0.956$		
	Γ_9^1	46.6	$c = 0.837$		
	Γ_7	0.8	$d = 0.548$		
	Γ_9^1	0.0			

[a] Eigenvector representation follows the conventions: $\Gamma_7 = |\pm^1/_2\rangle$; $\Gamma_8^1 = \mp a|\pm^5/_2\rangle \pm b|\mp^7/_2\rangle$; $\Gamma_8^2 = |b|\cdot|\mp^5/_2\rangle + |a|\cdot|\pm^7/_2\rangle$; $\Gamma_9^1 = \mp c|\pm^9/_2\rangle \pm d|\mp^3/_2\rangle$; $\Gamma_9^2 = |d|\cdot|\pm^9/_2\rangle + |c|\cdot|\mp^3/_2\rangle$.

The effect of the second term in eq 9 on the calculated heat capacity can be seen in Figure 1. Here the curve composed of the crosses is calculated for the CF parameters of scheme I using H_{dyn} = 500 kOe at 10 K. Although this value of H_{dyn} may be unrealistically high, it nonetheless indicates that an improvement in the quality of fit can be obtained by including dynamical exchange terms. It is impossible, however, on the basis of these data to determine whether the first, the second, or a combination of both explanations is the more appropriate for $NdAl_3$.

The calculated higher temperature heat capacity (Figure 2) needs no special comment since each scheme in Table I provides rather similar ΔC_p behavior for $T > 15$ K. The temperature position of the Schottky maximum corresponds with the experimental value of 35 K, and the general shape up to 80 K is reproduced. As has been mentioned, we were unable to rationalize the measured ΔC_p behavior above 100 K.

Some interesting distinctions between these sets of CF parameters are observed when calculating the thermal response of the CF entropy (Figure 5). Both schemes III and IV lead to a rapid accumulation of CF entropy between T_N and 6 K, whereas the entropy increment for the other schemes is more gradual and more consistent with experiment. The differences between the eigenvalues and eigenfunctions of the four possible parameter sets are shown in Table II. The existence of a low-lying first excited doublet in III and IV is the cause of their high entropy at low temperatures. We wish to avoid placing too much emphasis upon the discrepancy between these schemes (III, IV) and the experimentally obtained entropy since the latter quantity includes extrapolated values between 1.7 and 0 K. If one assumes that the real splitting between the ground and first excited states is indeed very small, then larger experimental entropy values than those allotted for by our extrapolation process would be observed below 1.7 K. Unfortunately, this temperature is the lowest obtainable with present equipment.

For the susceptibility calculations shown in Figure 3, the λ values were chosen so that the calculated curves would correspond with experiment over the widest temperature range. At higher temperatures curves I, III, and IV were so nearly coincident that they have been shown as a single line. This coincidence is extended to low temperatures and can only be distinguished in the enlarged graph between 2 and 16 K. Curve II represents the least accurate fit for the experimental

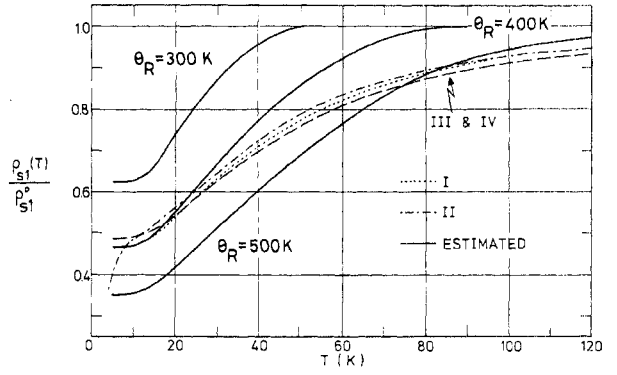

Figure 6. Comparison of the spin-disorder resistivity ratios for the schemes indicated. The estimated curves are derived from the experimentally measured resistivity using various approximations (θ_R) for the phonon contributions.

data through the whole temperature range. It is encouraging to note that part of the curvature in the measured $1/\chi$ curve at low temperatures can be explained on the basis of CF effects.

Finally, we interpret the effects of the crystal field on the measured resistivity in terms of a spin-exchange interaction involving the local moment–conduction electron system. This formalism[15] provides a temperature-dependent spin-disorder resistivity contribution [$\rho_{sl}(T)$] which is described by

$$\rho_{sl}(T) \propto \sum_{m_s, m_s', \Gamma_i, \Gamma_i'} \langle m_s', \Gamma_i' | s \cdot J | m_s, \Gamma_i \rangle^2 p_i f_{ii'} \qquad (10)$$

where m_s, Γ_i and m_s', Γ_i' are the initial and final conduction electron–local moment states, p_i is the Boltzmann population factor of the ith CF state, and $f_{ii'}$ is a function of the energy change associated with the scattering process. Because of the temperature dependence of $p_i f_{ii'}$, eq 10 approaches a constant value (ρ_{sl}°) for T much greater than the overall CF splitting temperature. The ratio $\rho_{sl}(T)/\rho_{sl}^\circ$, plotted in Figure 6, is equal to the right-hand side of eq 10. The corresponding experimental quantity is determined by subtracting the phonon (ρ_l) and residual (ρ_0) terms from the measured data. The latter has been estimated by extrapolation to T = 0 K, while we assume the former to follow a Grüneisen–Block type relationship[19]

$$\rho_l = \frac{KT}{\theta_R^2} G\left(\frac{\theta_R}{T}\right) \qquad (11)$$

Table III. Point Charge Calculation of the Effective Charge on the Aluminum Ions

Parameter and Scheme	No conduction electron shielding: Nearest neighbor (12 Al ions)[a]	No conduction electron shielding: Next nearest neighbors (12 Al + 8 Nd ions)[b]	Shell of radius a (30 Al + 14 Nd ions)[b]: $K = 0$	Shell of radius a (30 Al + 14 Nd ions)[b]: $K = 0.93$	Shell of radius $6a$ (8274 Al + 2902 Nd ions)[b]: $K = 0$	Shell of radius $6a$ (8274 Al + 2902 Nd ions)[b]: $K = 0.93$
B_2^0 I	+2.08	−5.03	−2.29	+2.51	−0.36	+2.13
B_2^0 II	−1.90	−12.79	+6.60	−3.92	−5.45	−3.50
B_2^0 III	−0.19	−9.47	+2.79	−1.69	−3.26	−1.06
B_2^0 IV	+0.09	−8.92	+2.16	−0.72	−2.91	−0.66
B_4^0 I	−5.12	−5.59	−5.28	−6.35	−4.39	−5.99
B_4^0 II	−4.88	−5.35	−5.03	−6.05	−4.20	−5.71
B_4^0 III	+1.76	+1.29	+1.73	+1.90	+1.25	+1.79
B_4^0 IV	+2.59	+2.12	+2.58	+2.88	+1.93	+2.72
B_6^0 I	−7.62	−7.42	−7.37	−10.6	−7.39	−10.6
B_6^0 II	+7.06	+7.26	+7.20	+10.1	+7.20	+10.6
B_6^0 III	+3.59	+3.76	+3.76	+5.21	+3.76	+5.21
B_6^0 IV	−3.26	−3.06	−3.04	−4.47	−3.05	−4.47

[a] $Z_{Al}(1 - \sigma_n)$. [b] Z_{Al} calculated using a value of +3 for Nd ions.

The constant K is obtained from the high-temperature experimental data and eq 11 is then solved for various values of θ_R. The resulting estimated $\rho_{sl}(T)/\rho_{sl}^{\circ}$ curves are also shown in Figure 6. Because of the uncertainty in θ the utility of the experimental results for comparison with theory is somewhat limited. Several reasonable values of θ have been chosen. As can be seen, for all values of the characteristic phonon temperature (θ_R) chosen, the estimated curves show a "flattening-off" of the resistivity ratio between 20 and 5 K. Calculations based on schemes I, III, and IV show this same feature; scheme II does not, suggesting it to be inapplicable. Mention should be made of the good fit of the remaining schemes to the estimated curve for $\theta_R = 400$ K between 5 and 30 K and the shift to the curve for $\theta_R = 500$ for $T > 70$ K. This confirms that the characteristic temperature θ_R is dependent on temperatures which can arise because of the changing importance with temperature of the Umklapp processes. This would lead to a significantly smaller θ_R at low T than at high T. One could thus envision a temperature-dependent $\theta_R(T)$ which would bring our calculated (I, III, and IV) and estimated [$400 \leq \theta_R(T) \leq 500$] curves into good agreement.

In view of the general interest in the classical electrostatic crystal field interpretation, we have examined the implications of our experimental parameters (Table I) in terms of the point charge model (PCM).[11,14] Based upon a Nd^{3+} ion, the PCM predicts the aluminum charge to have the values shown in Table III for (a) various extents of the lattice sum and (b) different estimations of the conduction electron shielding. The latter calculation employed a screened Coulomb potential approximation with a shielding parameter (K) very near that expected for a free-electron gas.[20] Additional calculations incorporating reasonable variations in the closed-shell shielding parameter, the conduction electron shielding parameter, and the charge on the neodymium ions provided no significant improvement in the values indicated in Table III. Clearly, only scheme III provides consistently positive values of Z_{Al} (we expect $Z_{Al} \approx +3$), and then only if the lattice sum is evaluated out to the specific value a. It appears that this correspondence is entirely coincidental and tends to conclude that the point charge approach represents an inacceptable modeling of the CF interaction in $NdAl_3$.

V. Conclusion

Interpretations of heat capacity, susceptibility, and resistivity data allow us to describe the crystal field interaction in $NdAl_3$ with three possible sets of parameters. Although each scheme may provide a satisfactory fit for a particular experimental measurement, no one scheme is clearly favored when considering the full variety of the data presented. Moreover, the CF interaction cannot be satisfactorily interpreted on the basis of the point charge model. A sizable contribution of the CF seems to come from nonelectrostatic origins. It is likely that the present data can be made use of in developing a suitable theoretical basis for the CF interaction. A necessary preliminary to this will be the selection of a single set of W, x, and y parameters appropriate for all the observed quantities. This, of course, was the intended goal of our investigation. Various limitations in the extraction of crystal field dependent quantities from the measurements prevent the achievement of this goal. Inelastic neutron-scattering experiments planned for the near future may enable the relevant parameters to be established unambiguously.

Acknowledgment. This work was supported by a grant from the U.S. Army Research Office—Durham. J.V.M. wishes to thank his colleagues in the "Delegation für Ausbildung und Hochschulforschung" at the Eidgenössisches Institut für Reaktorforschung, Würenlingen, Switzerland, for creating the stimulating environment which so greatly helped the completion of this paper.

Registry No. $NdAl_3$, 12043-38-8; $LaAl_3$, 12043-35-5.

References and Notes

(1) R. D. Hutchens and W. E. Wallace, *J. Solid State Chem.*, **3**, 564 (1971); W. E. Wallace, *Prog. Solid State Chem.*, **6**, 155 (1971); R. S. Craig, S. G. Sankar, N. Marzouk, V. U. S. Rao, W. E. Wallace, and E. Segal, *J. Phys. Chem. Solids*, **33**, 2267 (1972); N. Marzouk, R. S. Craig, and W. E. Wallace, *ibid.*, **34**, 15 (1973); S. G. Sankar, D. Keller, R. S. Craig, W. E. Wallace, and V. U. S. Rao, *J. Solid State Chem.*, **9**, 78 (1974); R. D. Hutchens, W. E. Wallace, and N. Nereson, *ibid.*, **9**, 152 (1974); D. A. Keller, S. G. Sankar, R. S. Craig, and W. E. Wallace, *AIP Conf. Proc.*, **No. 18**, 1207 (1974).
(2) J. E. Greedan and V. U. S. Rao, *J. Solid State Chem.*, **6**, 387 (1973).
(3) S. G. Sankar, V. U. S. Rao, E. Segal, W. E. Wallace, W. Frederick, and H. Garrett, *Phys. Rev. B*, **11**, 435 (1975).
(4) A. Furrer, W. Bührer, H. Heer, H.-G. Purwins, and E. Walker, *Int. J. Magn.*, **4**, 63 (1973).
(5) J. V. Mahoney, unpublished work.
(6) J. V. Mahoney, W. E. Wallace, and R. S. Craig, *J. Appl. Phys.*, **45**, 2733 (1974).
(7) J. V. Mahoney, V. U. S. Rao, W. E. Wallace, and R. S. Craig, *Phys. Rev. B*, **9**, 154 (1974).
(8) K. H. J. Buschow and J. F. Fast, *Z. Phys. Chem. (Frankfurt am Main)*, **50**, 1 (1966).
(9) J. V. Mahoney, Ph.D. Thesis, University of Pittsburgh, 1972.
(10) R. S. Craig, S. Nasu, and H. H. Neumann, to be submitted for publication.
(11) See, for example, W. E. Wallace, "Rare Earth Intermetallics", Academic Press, New York, N.Y., 1973, Chapter 3.
(12) J. H. N. van Vucht and K. H. J. Buschow, *J. Less-Common Met.*, **10**, 98 (1965).
(13) K. R. Lea, M. J. M. Leask, and W. P. Wolf, *J. Phys. Chem. Solids*, **23**, 1381 (1962).
(14) M. T. Hutchings, *Solid State Phys.*, **16**, 227 (1964).
(15) V. U. S. Rao and W. E. Wallace, *Phys. Rev. B*, **2**, 4613 (1970).
(16) Y.-L. Wang and B. R. Cooper, *Phys. Rev. B*, **2**, 2607 (1970).
(17) D. J. Newman, *Adv. Phys.*, **19**, 198 (1971).
(18) A. Furrer and H. Heer, *Phys. Rev. Lett.*, **31**, 1350 (1973).
(19) G. T. Meaden, "Electrical Resistance of Metals", Plenum Press, New York, N.Y., 1965.
(20) U. Tellenbach, Report AF-SSP-76, EIR, Würenlingen, Switzerland, 1974.